J. Fluid Mech. (1985), *vol.* 150, *pp.* 281–309
Printed in Great Britain

The plane turbulent shear layer with periodic excitation

By H. E. FIEDLER AND P. MENSING†
Herman-Föttinger-Institut für Thermo- und Fluiddynamik, Technische Universität Berlin

(Received 10 December 1982 and in revised form 17 May 1984)

The influence of periodic excitation on a plane turbulent one-stream shear layer with turbulent separation was investigated. For the qualitative study flow visualization was employed. Quantitative data were obtained with hot-wire anemometry and spectrum analysis. It was found that sinusoidal perturbations with frequencies of order $f_0 \lesssim u_0/100\theta_0$ (depending on excitation strength), introduced at the trailing edge are always amplified. Maximum amplification factors are observed for the lowest perturbation levels. The frequency and amplitude of excitation determine the downstream location of the amplification maximum in the flow. At sufficient amplitude two-dimensional vortices are formed which subsequently decay without pairing. The development of the periodic r.m.s. values along x follows a universal curve for all frequencies and amplitudes when properly normalized.

At high excitation amplitudes the flow development depends strongly on the geometrical conditions of the excitation arrangement at the trailing edge. Thus regular vortex pairing as well as suppression of pairing can be achieved.

The excited shear layer has considerably stronger, yet nonlinear, spread than the neutral. The region of vortex formation, irrespective of whether it includes pairing or not, is associated with a step-like increase in width, while after the position of maximum vortex energy, i.e. in the region of decay, the spread is reduced to values below the neutral. There the overall lateral fluctuation energy is increased, while the longitudinal may be decreased as compared with the neutral flow.

1. Introduction

Periodically excited free shear flows tend to roll up into discrete vortices whose shape and strength depend on the type of flow considered, its boundary conditions and the excitation amplitude. This phenomenon, first reported in the nineteenth century, is generally associated with laminar flow. Michalke (1971) showed that inviscid stability theory appears to be applicable also to turbulent flow. The concept of coherent structures, which emerged at about the same time, is essentially based on the inherent large-scale instability of the turbulent flow and the subsequent formation of discrete modules, the coherent structures, whose initiation and strength is, however, not yet fully assessed, even for such simple cases as the neutral shear layer.

In order to quantify the influence of defined periodic perturbations on a plane shear layer and at the same time obtain information about formation and characteristics of coherent structures under defined circumstances, the following investigation was undertaken. The results reported herein are largely based on the dissertation of the second author (Mensing 1981).

† Present address: Amt für Umweltschutz, Hamburg.

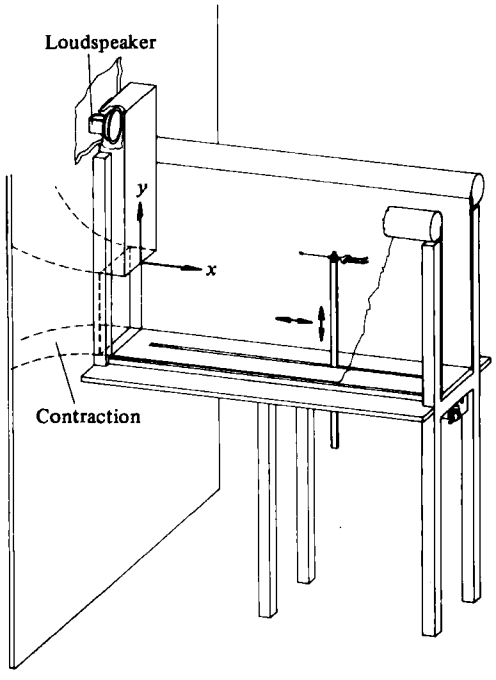

FIGURE 1. Test section and coordinate system.

2. Experiments

2.1. *General arrangement and initial conditions*

This investigation was first started in a blowing facility. It was, however, found that the shear layer then investigated was to some extent disturbed by periodicities apparently caused by the blower as well as by the settling tube, acting as an organ pipe. This was surprising, since these perturbations were too weak to appear in the spectrum of the free-stream turbulence in the nozzle exit.

A new facility was then designed where a contraction with a cross-section of 300×300 mm at the exit is placed between two rooms, which are kept at different pressure levels. Upstream of the nozzle a basket-like foam-rubber screen is placed around the intake. The test section mounted at the nozzle exit has a length of 1260 mm. It is fitted with glass walls and rounded corners at the open upper side to ensure smooth entrainment flow. The turbulence level in the nozzle is $< 0.15\,\%$, with no single frequency in the spectrum discernible. Figure 1 shows the complete arrangement and the coordinate system used.

The separating boundary layer at the trailing edge was tripped 100 mm upstream of the trailing edge by a strip of coarse sandpaper of 40 mm width. Chosen according to Smith & Clutter (1957), it causes fast transition with no prevailing periodic constituent in the fluctuation spectrum. The boundary-layer profile at the trailing edge is shown in figures 2 (a,b). It corresponds essentially to a boundary-layer profile with slight adverse pressure gradient, having a momentum thickness of $\theta_0 = 1.14$ mm and a form parameter of $H = 1.46$ (see also Hussain & Zedan 1978a,b). According to Bradshaw's (1966) criterion, most of the flow in the test section may not be considered fully self-preserving. Newer evidence suggests, however, a shorter length for the structural development of the flow, so that approximately the second half of

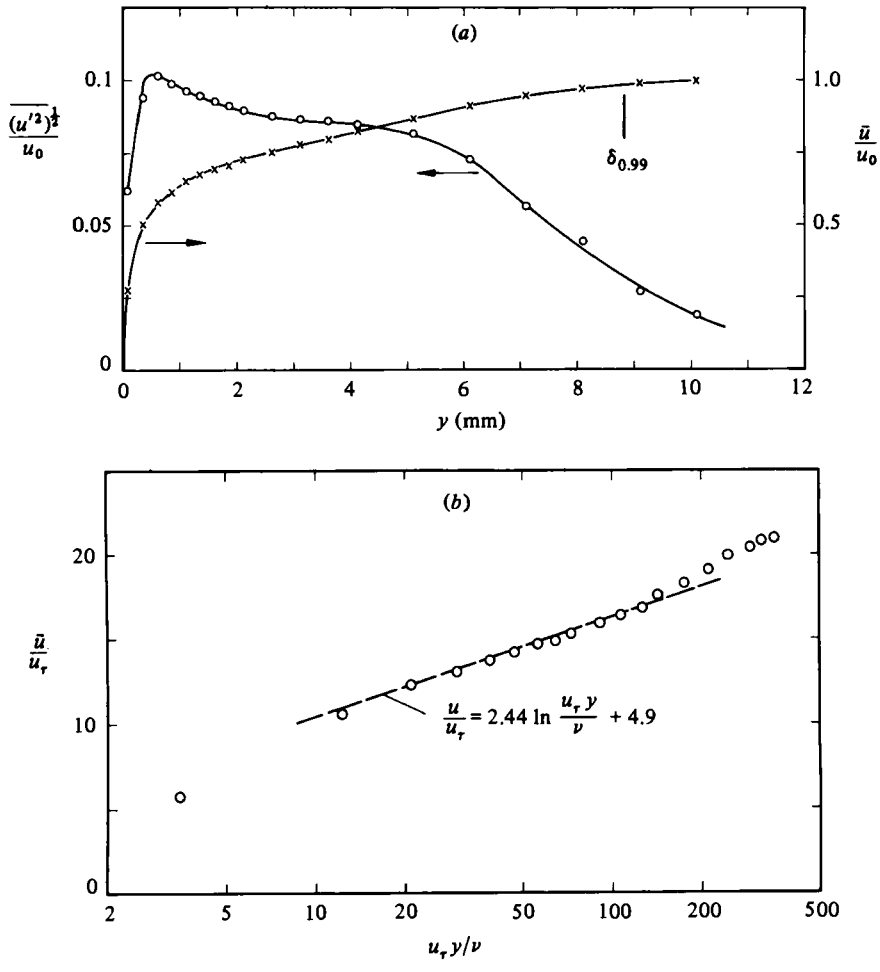

FIGURE 2. (*a*) Mean-velocity and u' distributions of separating turbulent boundary layer. (*b*) Logarithmic plot of separating boundary layer.

the shear layer will essentially be self-preserving. For the excited flow this limit is, however, of little relevance. There the thickness of the separating boundary layer is primarily important in providing an upper bound for the excitation frequencies (see §3.2.3).

All measurements reported were done with DFVLR hot-wire equipment. Spectra were obtained with a Hewlett-Packard 3582A analyser.

2.2. *Experimental conditions*

In discussing free-shear-layer flow we refer to three conditions: neutral flow, disturbed flow and excited flow. A *neutral* condition is assumed when in no position in the flow are isolated spectral peaks found. *Disturbed* flow denotes the case where no periodic constituent is observed in the free-stream turbulence in the beginning of the test section, yet isolated spectral peaks of constant, i.e. x-independent, frequency develop downstream (facility forcing). Finally, *excited* flow describes the situation where periodic disturbances of defined frequency and amplitude are imposed on the

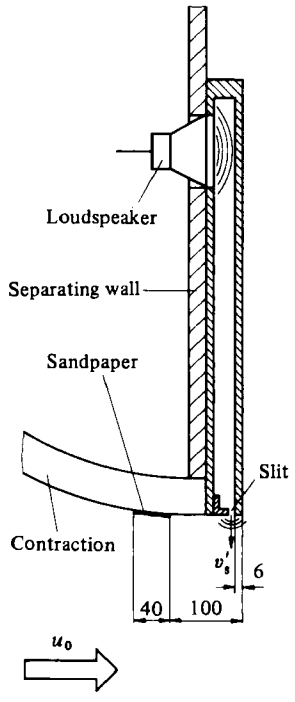

FIGURE 3. Loudspeaker arrangement at trailing edge (see also figures 8 and 9).

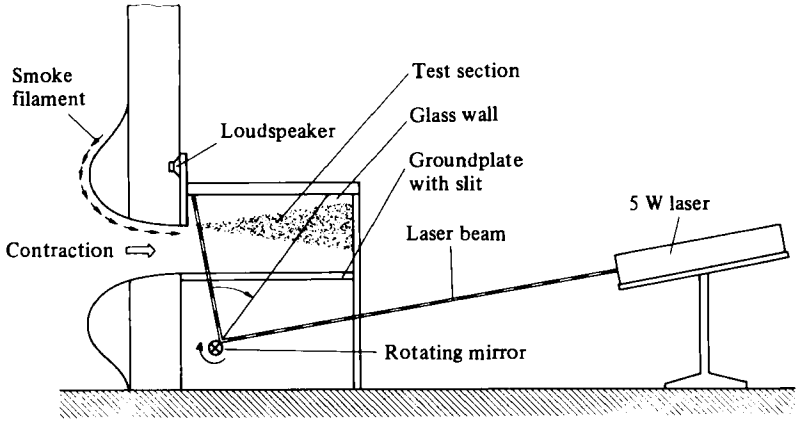

FIGURE 4. Flow-visualization arrangement.

flow, in particular at the trailing edge. Regarding the flow behaviour, there is only a quantitative distinction between the latter two conditions. The basic requirement for an investigation of excited flow must, however, be the neutral condition, since otherwise mixed conditions in phase or frequency may occur. In the present test arrangement, standing waves in the test room were observed at certain blower speeds, causing a flow disturbance. Perfectly neutral flow was found only for $u_0 = 11$ m/s. All measurements were carried out at this velocity. It corresponds to a Reynolds number $Re_x = xu_0/\nu = x \times 7.3 \times 10^3$ (x in cm).

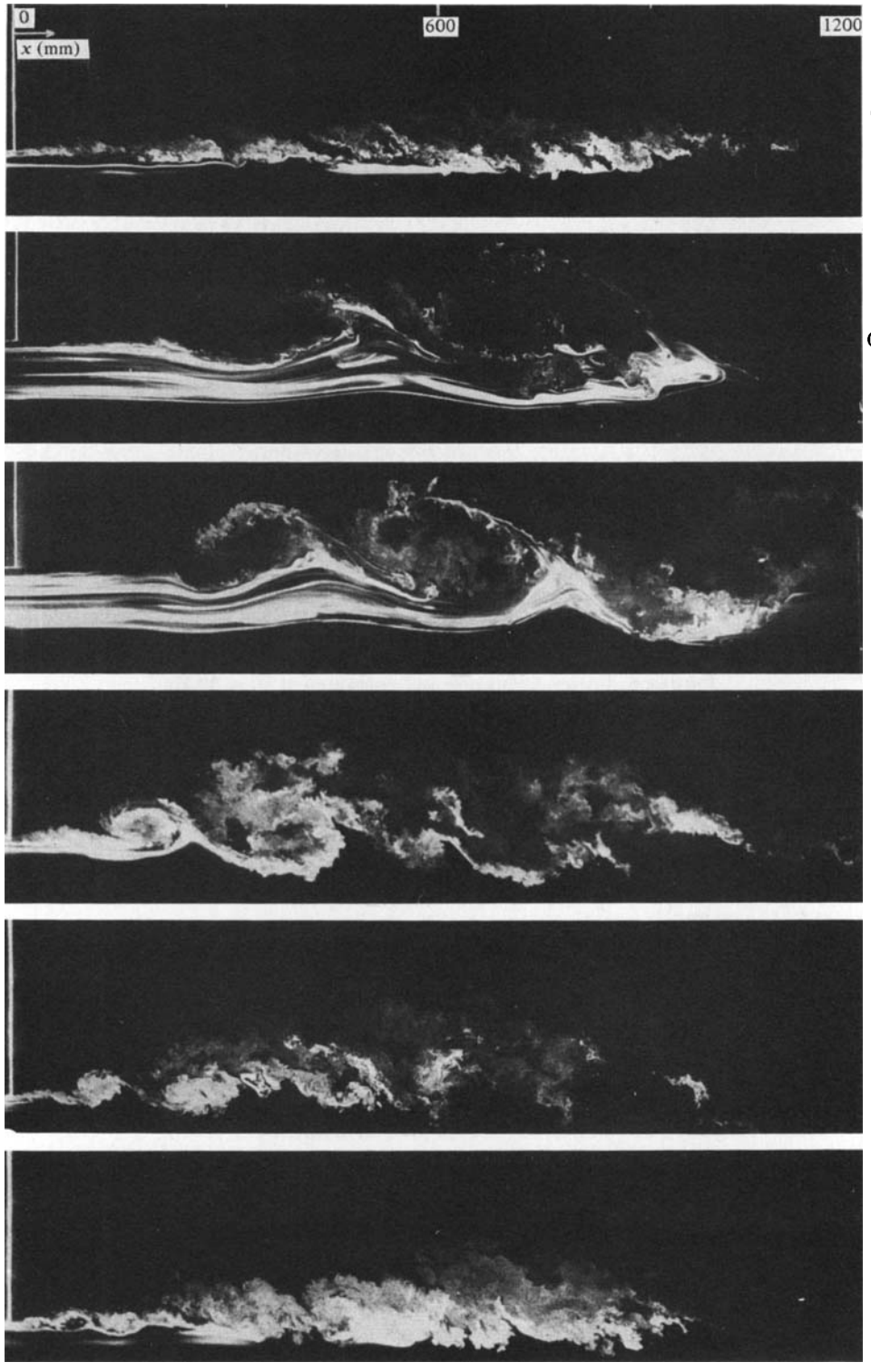

FIGURE 5. Vortex development for various excitation frequencies and $(v_{p0})'/u_0 = 0.0065$: (*a*) 0 Hz (neutral case); (*b*) 20 Hz; (*c*) 30 Hz; (*d*) 40 Hz; (*e*) 60 Hz; (*f*) 110 Hz.

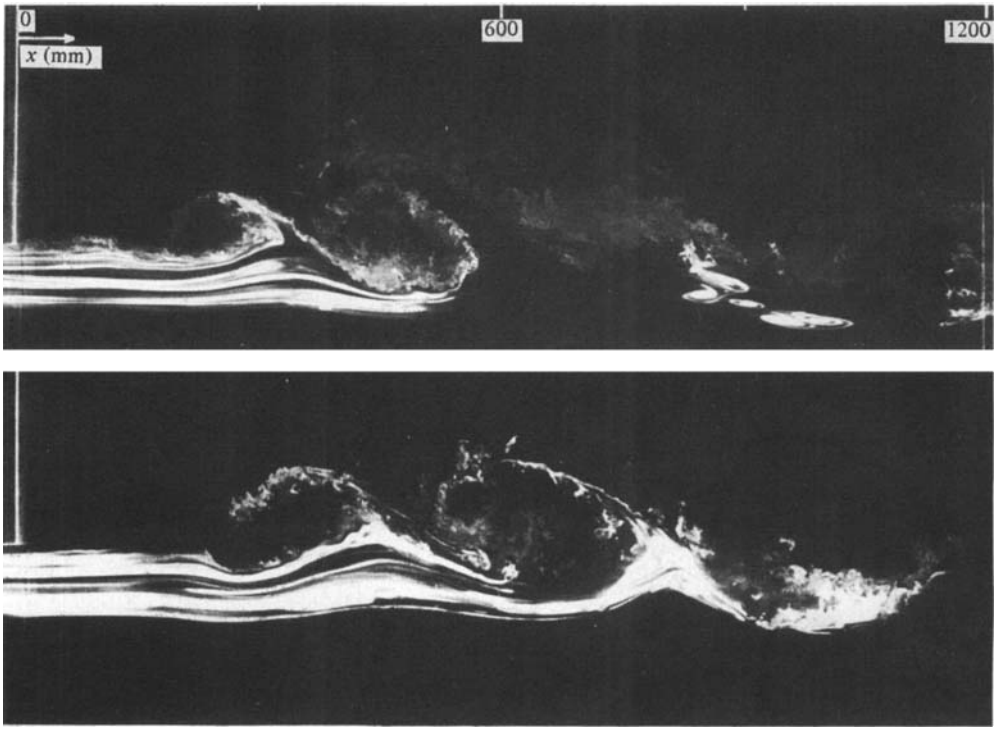

FIGURE 6. Vortex formation and entrainment ($f_0 = 30$ Hz).

2.3. *Flow excitation*

Of the many possible ways to introduce defined periodic perturbations into the flow, some of which were discussed by Korschelt (1980), excitation by loudspeaker was chosen, the arrangement of which is sketched in figure 3. The particle velocity v_s' in the slit, caused by the pumping action of the speaker, modulates the separating boundary layer. This technique is probably the most simple one, allowing easily for a large and repeatable range of amplitude and frequency, while being perfectly two-dimensional. For studies of the flow immediately downstream of the trailing edge it must, however, be considered with caution, since in addition to deflecting the boundary layer it also introduces a pulsating mass flow.

2.4. *Visualization*

The method employed in this study, described in detail by Mensing & Fiedler (1980), utilizes a focused laser beam of 5 W, which is scanned through the test section by a rotating mirror. For a typical time $\Delta t = 0.01$ s for the laser beam to sweep the test section of length L, a beam width of, say, 3 mm and a flow velocity of 11 m/s, an individual smoke particle travels approximately 0.3 mm during its illuminated time. The camera, whose shutter speed may be $\frac{1}{30}$ s, is triggered by a photocell. In this way sharp pictures of the flow structure down to its smallest elements are obtained. The overall flow image, however, appears compressed or expanded, depending on the sweep direction, by some 5%. Figure 4 shows the arrangement.

Flow photographs were taken in a neutral shear layer, a weakly excited flow and a flow with strong excitation. They are shown on figures 5–10. Before discussing the

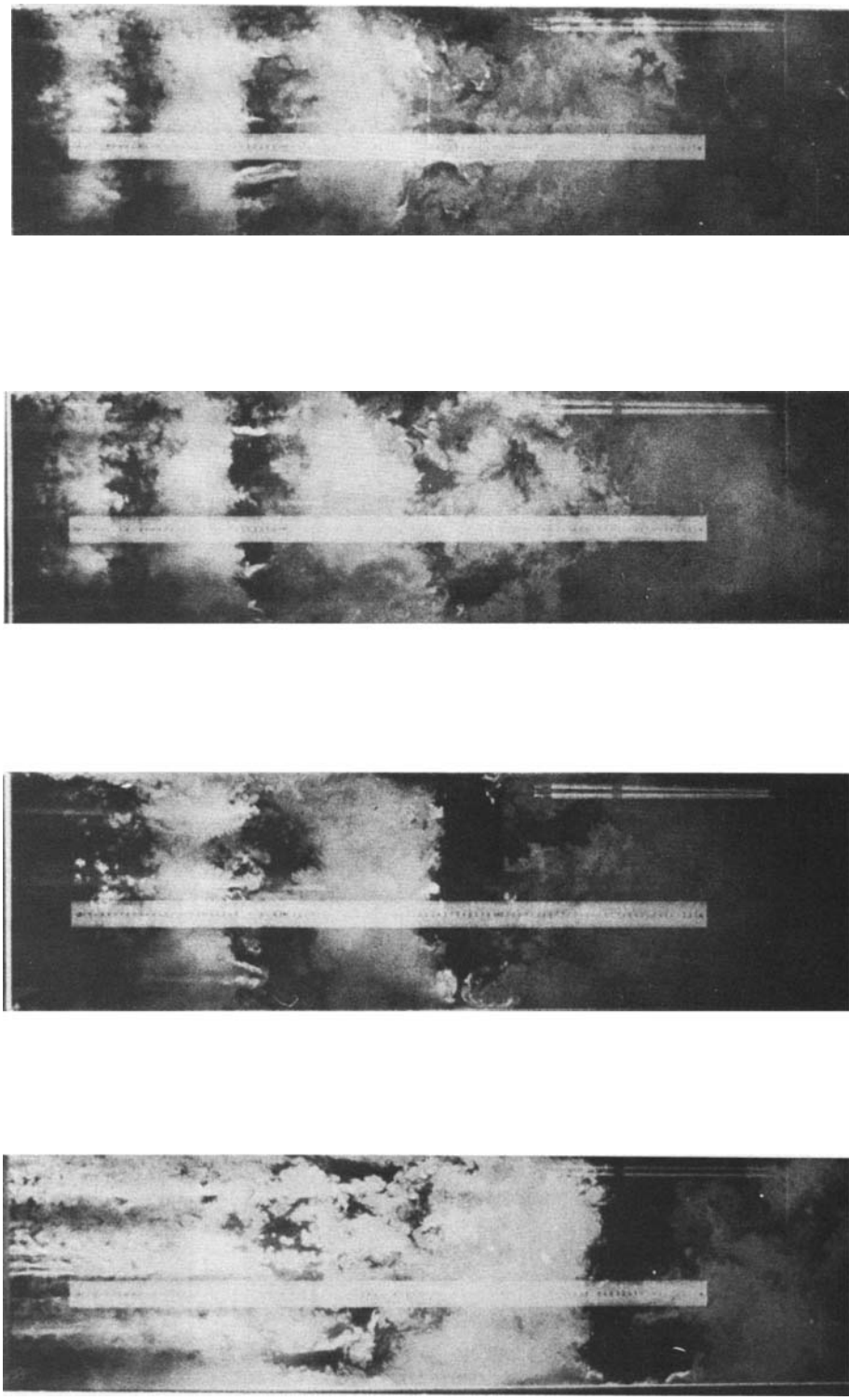

FIGURE 7. Two-dimensionality of excited structures: (*a*) 30 Hz; (*b*) 30 Hz; (*c*) 20 Hz; (*d*) 15 Hz.

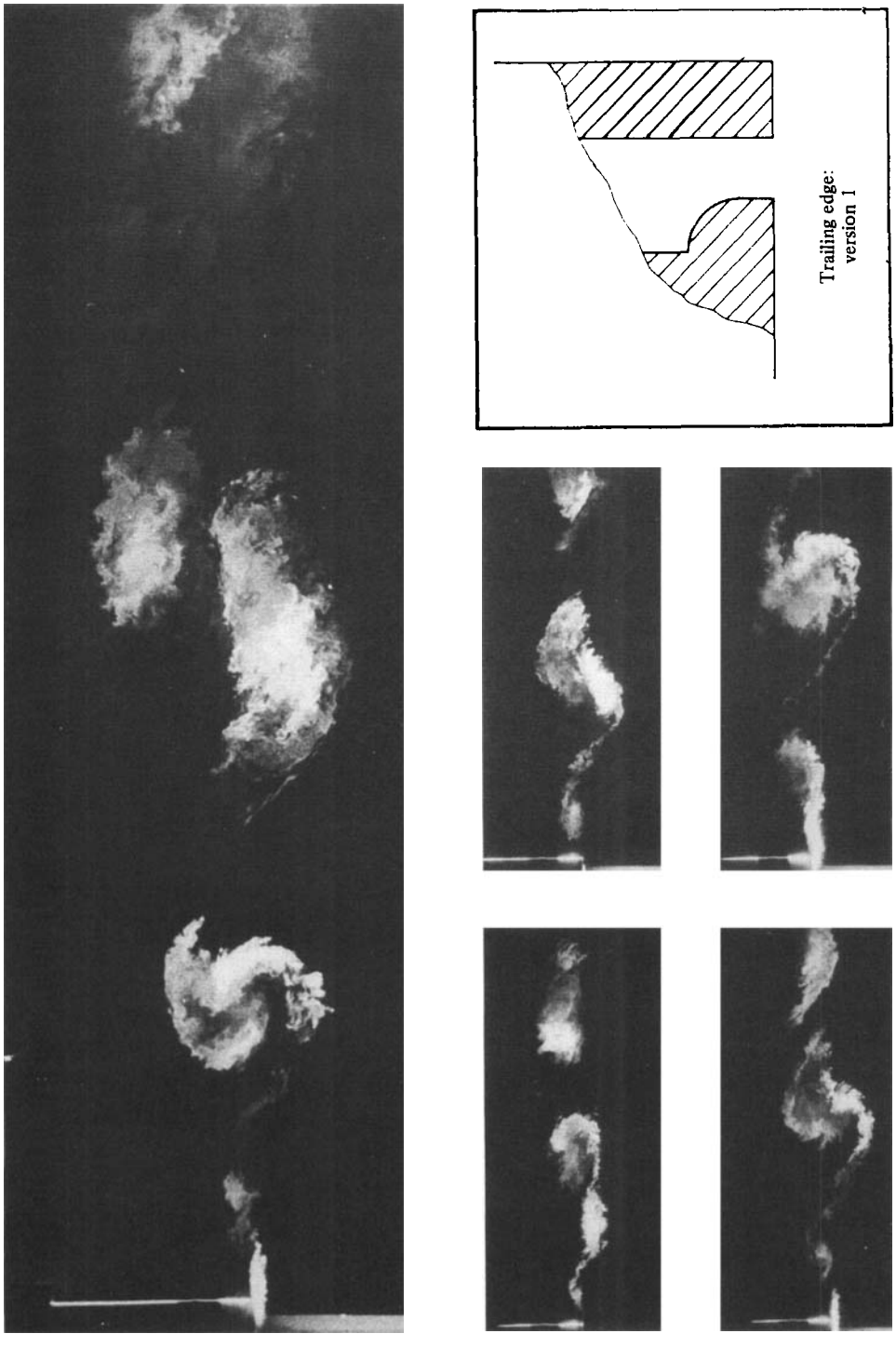

FIGURE 8. Overall flow development with pairing and enlarged sequences of flow near trailing edge with preceding pairing: strong excitation with disturbed separation conditions.

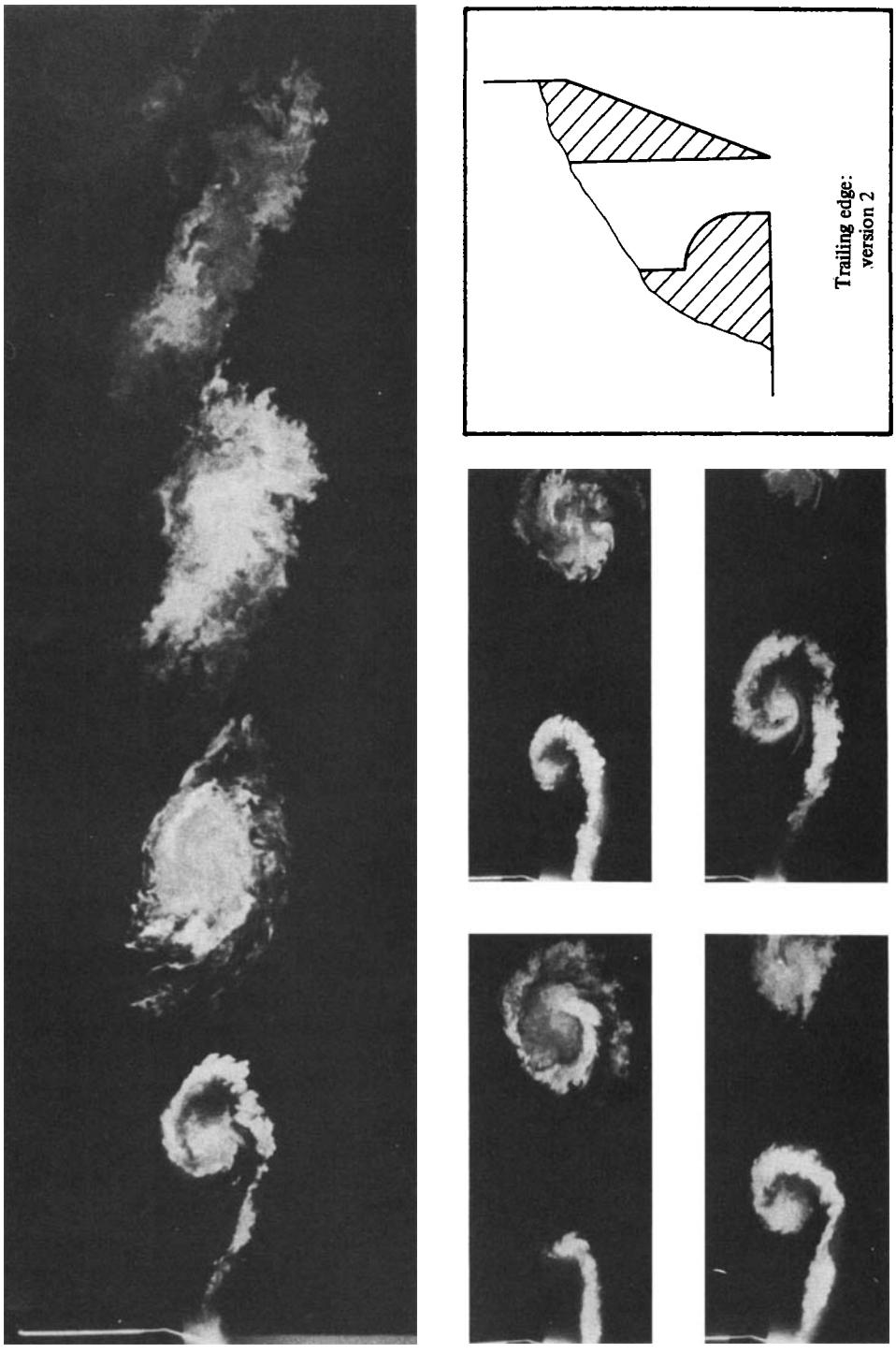

FIGURE 9. Overall flow development without pairing and enlarged sequences of flow near trailing edge: strong excitation with clean separation condition.

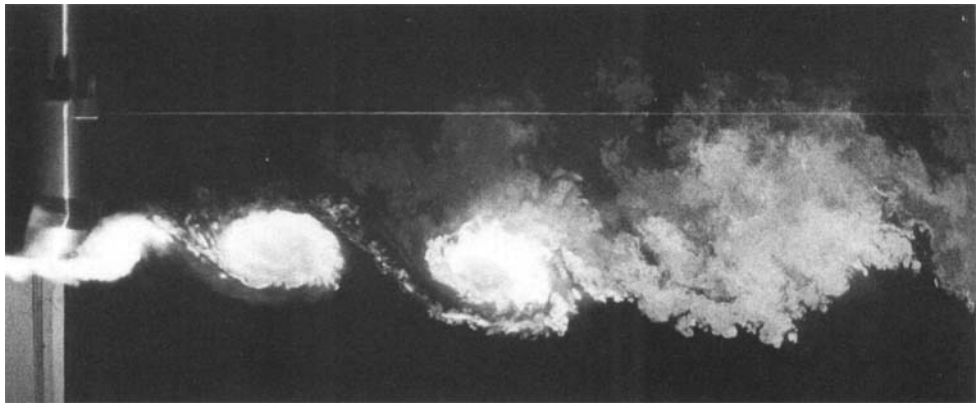

FIGURE 10. Flow development at strong excitation and clean separation showing sudden diffusion and vortex breakup.

flow development together with the supporting measurements in detail we may obtain a qualitative picture of the excited flow. Obviously the excitation leads to the formation of strong discrete vortices following a region where the imposed vertical excursions are amplified and cause the shear layer to undulate. The vortices in their final state appear to be stable only for a short time. In due course they lose coherence and are either predominantly torn at weak excitation or may undergo a pairing process at strong excitation (see also Fiedler *et al.* 1981). The artificially triggered structures are approximately two-dimensional, spanning the width of the test section (figure 7).

The smoke may be introduced into the flow through the loudspeaker slit (figures 8–10). This method, however, has the disadvantage of strong dilution of the smoke by the entrained fluid, which renders photography in the downstream region difficult. For a number of photographs we have therefore introduced the smoke far upstream of the trailing edge at the beginning of the contraction, so that the smoke trail is carried in the potential fluid, feeding the turbulent regime by entrainment along x (figures 5–7).

3. Results: structural (periodic) quantities

3.1. *Neutral flow*

Figure 5(a) juxtaposes this case against the excited cases. Clearly the neutral flow has a smaller spread angle and the structures do not appear to be clearly defined. They are rather lumpy and irregular and show little resemblance to the ones observed, for example, by Brown & Roshko (1974). This difference may be attributable to the different visualization techniques used. According to Wei, Niu & Ma (1982); however, those structures should not appear for $Re^* = \delta_0 u_\tau/\nu > 34$ (in our case $Re^* = 350$). This criterion is, however, not conclusive, since it was obtained for a low-Re case. Structures of the kind observed may still be quite coherent and two-dimensional, as was observed by Browand & Troutt (1980).

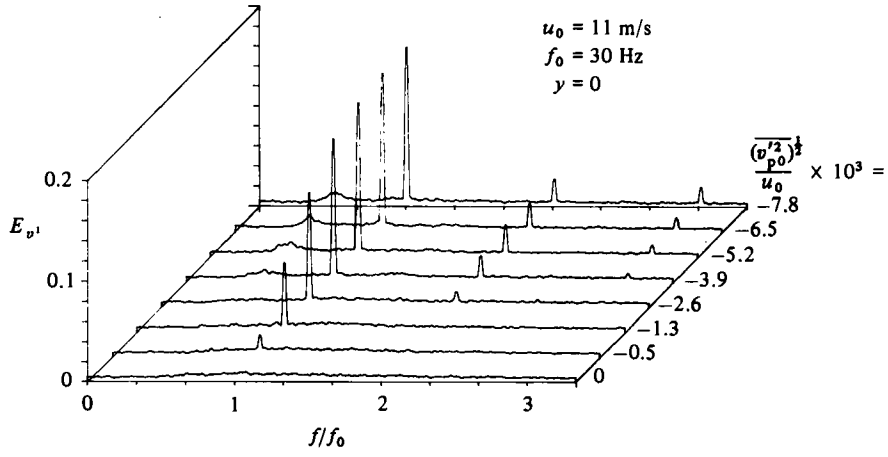

FIGURE 11. v' spectra for different excitation amplitudes at $S_x = 1$.

3.2. *Excited flow*

3.2.1. *Choice of frequency*

Most measurements presented were obtained at excitation frequency $f_0 = 30$ Hz. Since the turbulent shear layer is a self-similar flow (except in the dissipation range) with no distinguished lengthscale and with a characteristic frequency $f_c \sim u_0/(x-x_0)$, the reaction of the flow to periodic excitation of a certain amplitude must be independent to the frequency when plotted versus a normalized abscissa (Strouhal number)

$$S_x = (x-x_0^*)\, f_0/u_0,$$

where f_0 is the excitation frequency and x_0^* a virtual origin, which is not the same as in the neutral case, but independent of frequency at a given amplitude. Thus the flow is not frequency-selective and for each frequency the degree of randomization of the driving wave at the position of maximum amplification is the same. This proposition is clearly proven by a number of measurements at different frequencies and in particular by the identity of the normalized amplification curve for different frequencies as shown in figure 15.

3.2.2. *Amplification at different initial amplitudes*

The amplification of a periodic perturbation along the flow was studied by spectral analysis of the v' signal along the x-axis, and for some cases in the whole flow field. The lateral fluctuation was considered to be of particular interest, since the initial perturbation was lateral and it is mainly this fluctuation that reflects the strength of the large vortices in the flow centre. A typical example for the spectra E_v as obtained for different excitation amplitudes at $S_x = 1$ (where approximately maximum amplification is achieved) is shown in figure 11.

For a direct assessment of the periodic constituent the turbulent signal is decomposed into a stochastic and a periodic part:

$$v' = v'_s + v'_p, \quad \text{and thus} \quad \overline{v'^2} = \overline{v'^2_s} + \overline{v'^2_p}.$$

Local periodic intensity is then obtained by subtraction of the stochastic background energy from the peak energy of the spectrum. In the following only the periodic signal content is considered.

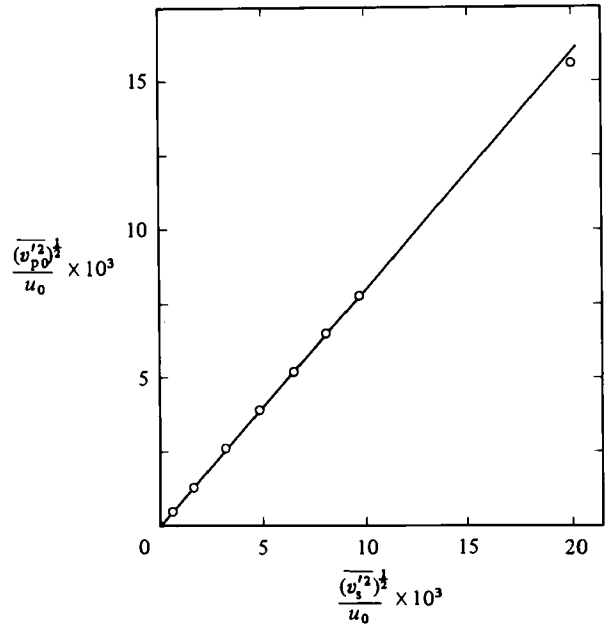

FIGURE 12. Excitation amplitude versus particle velocity in loudspeaker slit at zero flow velocity.

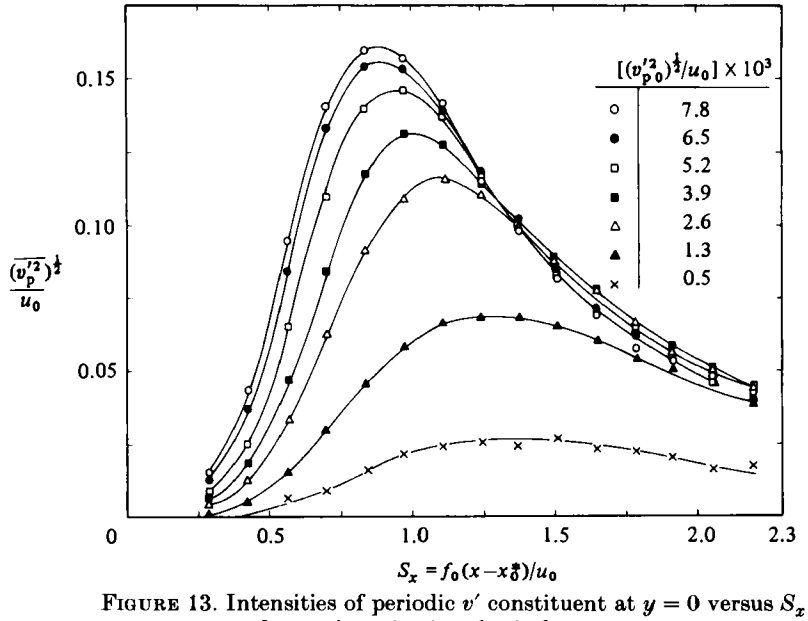

FIGURE 13. Intensities of periodic v' constituent at $y = 0$ versus S_x for weak excitation: basic frequency.

The initial excitation strength $(v_{p0})'$ was determined by cross-correlation of the speaker input with the hot-wire signal in the boundary layer at $x = 0$ and the y-position of maximum correlation, since these fluctuations – at least for weak excitation – appear to be fully embedded in the random turbulence of the separating boundary layer.

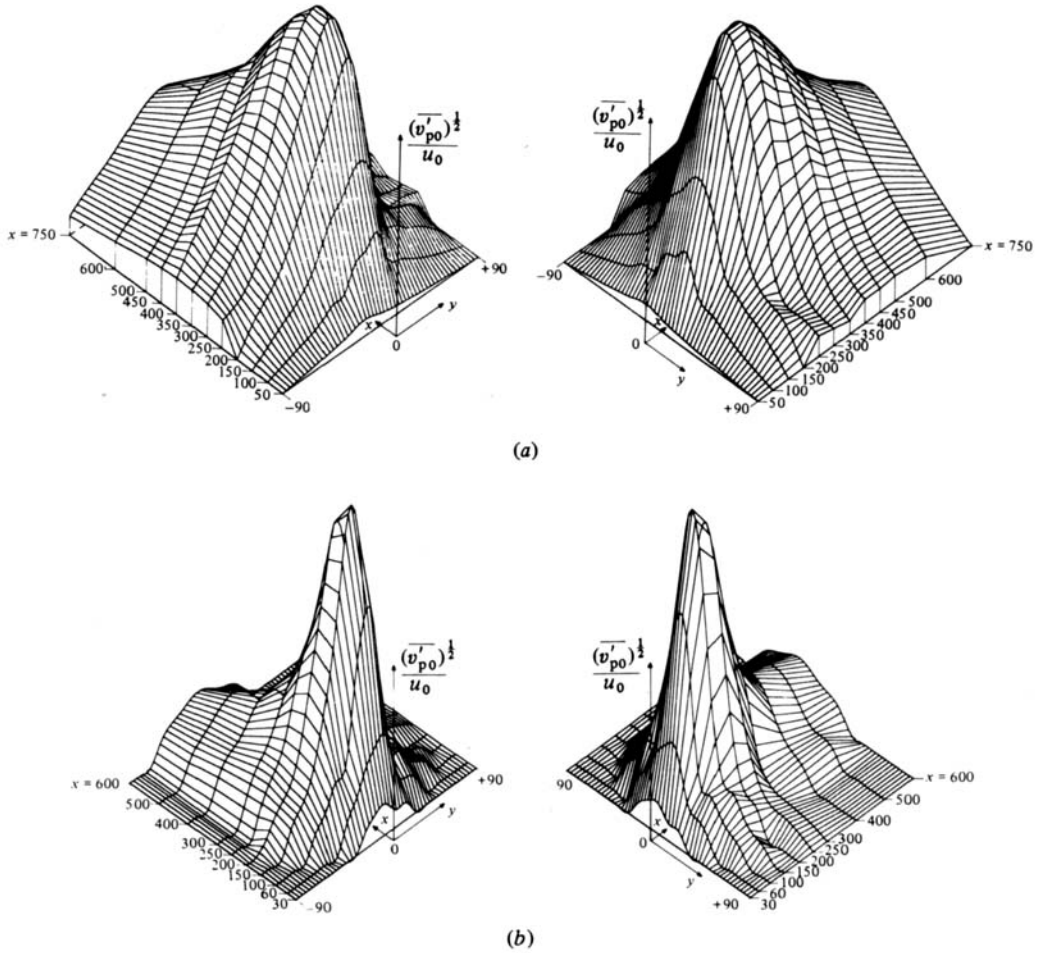

FIGURE 14. (*a*) Spatial distribution of periodic v' constituent at $f_0 = 30$ Hz. (*b*) Spatial distribution of periodic v' constituent at $f_0 = 50$ Hz.

The symbol ( )′ is used in the following for r.m.s. values and the averaged shear stress.

Although the values thus obtained appear to be most appropriate for scaling, since they truly represent the initial excitation amplitude at working condition, the particle velocity in the slit of the loudspeaker system was also measured for $f_0 = 30$ Hz at corresponding speaker voltages but with the flow turned off. The comparison is presented in figure 12. Obviously there is perfect correlation between the two parameters at 'weak' excitation, with the 'true' initial amplitude being 20 % smaller than the amplitude of the particle velocity.

Weak excitation. The main part of the investigation was concerned with the weakly excited flow, i.e. $(v_{p0})'/u_0 \leqslant 0.0078$. For this situation figure 13 shows the development of the periodic signal intensity at $y = 0$ versus S_x for various excitation amplitudes. Since, in spite of the unequal spreading of the shear layer on the two sides, the locations of the maxima of the lateral $(v_p)'$ distributions are essentially at $y = 0$ (see also figures 14(*a*,*b*) and 31), the distributions in figure 13 give the longitudinal development of the maximum value of $(v_p)'$. At $S_x = 1$ (depending on excitation

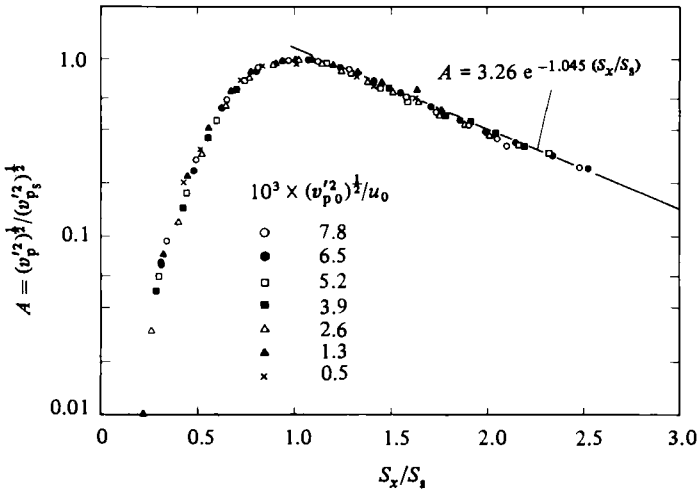

FIGURE 15. Universal excitation curve of periodic v' constituent at $y = 0$ for various excitation amplitudes (and various frequencies).

strength) the curves reach a maximum which corresponds to the position of strongest development of the vortices. The distance from the trailing edge to the location of the maximum is denoted by x_s, and we define a saturation Strouhal number

$$S_s = (x_s - x_0^*) f_0/u_0.$$

Figures 14(*a*,*b*) show spatial distributions of the spectral peak envelopes for two frequencies, demonstrating perfect similarity.

Closer inspection of figure 7 discloses a similarity of the amplification curves for the various excitation levels. Indeed, by proper normalization the curves can be made to collapse on to a single one with remarkably little scatter. Figure 15 gives the universal amplification curve, which is independent of amplitude and frequency. It may be approximated by

$$A = \frac{(v_p)'}{(v_{p,\max})'} = 20\left(\frac{S_x}{S_s}\right)^4 \exp\left(-3\frac{S_x}{S_s}\right),$$

where

$$\frac{S_x}{S_s} = \frac{f}{f_0}\bigg|_{x=\text{const}} = \frac{x}{x_s}\bigg|_{f=\text{const}}.$$

Considering only the decaying part of the curve, we may write

$$A = 3.26 \exp\left(-1.045\frac{S_x}{S_s}\right).$$

This gives an idea of the longevity of a disturbance. We find that only at $S_x/S_s = 3.3$ has the periodic intensity constituent decayed to 10% of its maximum value.

From determination of x_s for different frequencies f_0 and constant amplitudes the actual virtual origin x_0^* is obtained (figure 16). The maxima in figure 13 increase with increasing excitation amplitude, while the amplification factor

$$k = (v_{ps})'/(v_{p0})'$$

versus excitation intensity, as plotted in figure 17, decreases. It is largest for $(v_{p0})' \to 0$, where $k \approx 53$. This is of some interest, as it explains why the extremely weak

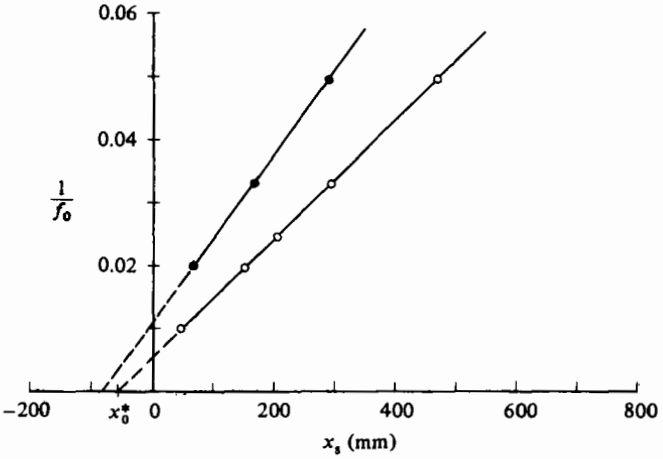

FIGURE 16. Saturation length versus excitation frequency; evaluation of x_0: ○, $(v_{p0})'/u_0 = 0.0065$; ●, 0.065.

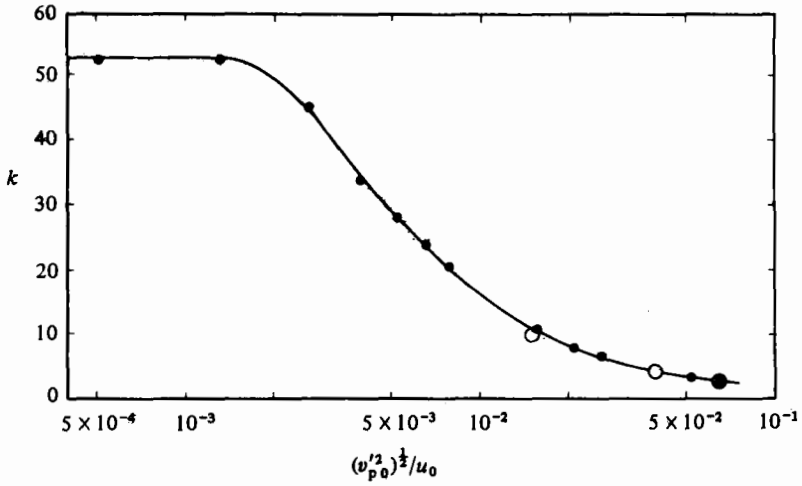

FIGURE 17. Amplification factor versus excitation amplitude.

disturbances, as, for example, from blower periodicity or organ-pipe resonance, may have a remarkable effect on the flow development.

Strong excitation. In this situation it seemed to be of interest to investigate the possibility of an asymptotic value for the maximum periodic energy in the shear layer at high excitation. Figure 18 shows some amplification curves for excitation amplitudes of up to $(v_{p0})'/u_0 = 0.065$. We observe a comparatively weak further growth of the maximum accompanied by its further shift upstream. In the decay range the curves deviate considerably from those at small amplitudes.

Smoke photographs of the flow at strongest excitation show a sequence of pairings, leading to formation of the vortices of basic (f_0) and of subharmonic ($\frac{1}{2}f_0$) frequency (figure 8). Formation of the primary vortices of frequency $2f_0$ is apparently caused by the particular excitation arrangement used. At strong excitation the flow separates upstream of the trailing edge during a 'pumping' cycle. At reattachment then a starting vortex is formed, which moves with retarded speed. It is quickly

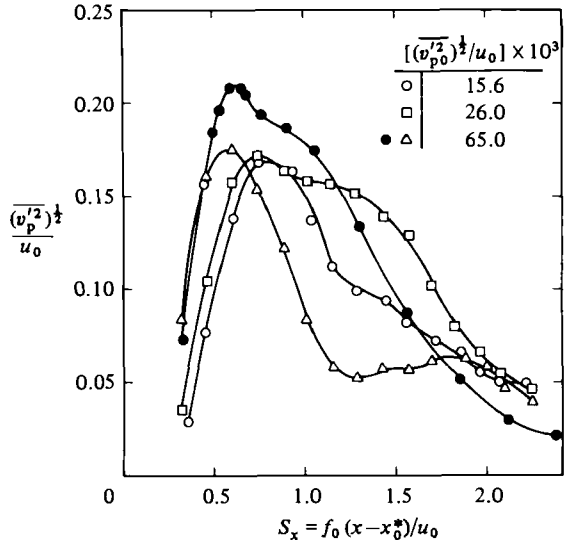

FIGURE 18. Intensities of periodic v' constituent at $y = 0$ versus S_x for strong excitation: basic frequency.

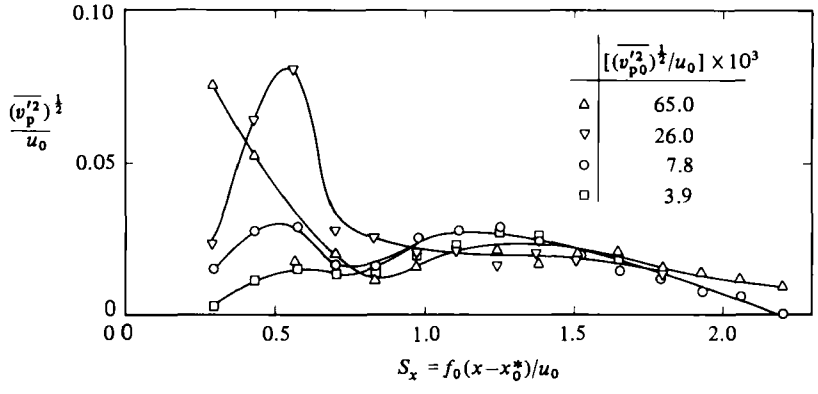

FIGURE 19. Intensities of periodic v' constituent at $y = 0$ versus S_x: 1st harmonic.

overturned by the following 'triggered' vortex and in due course amalgamated, thus forming the basic vortex. This first pairing occurs only at strong excitation amplitudes. It is significant for the further development of the flow, as it is responsible for the subsequent pairing of vortices of basic frequency, which is not observed at weak excitation. By sharpening the coverplate of the loudspeaker box at the trailing edge, pairing can be completely suppressed for all excitation amplitudes studied. In this situation then the basic vortices at strong excitation are strongly stabilized. They exist over a region of more than twice their diameter downstream, followed by a rather sudden disintegration (figure 10).

The two different situations are demonstrated by the flow pictures on figures 8 and 9. The flow at the 'clean' separation condition appears to be only quantitatively different from the weakly excited case. The 'disturbed' separation, on the other hand, has a different quality. It provides a possibility for studying stabilized vortex pairing. In the following discussion primarily the latter case is referred to. Only a few measurements obtained with clean separation are included in some of the figures.

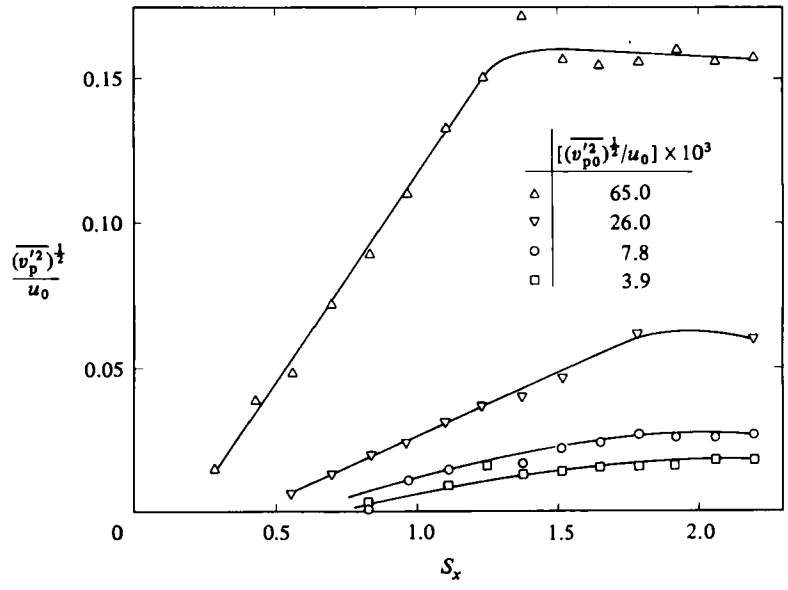

FIGURE 20. Intensities of periodic v' constituent at $y = 0$ versus S_x: subharmonic.

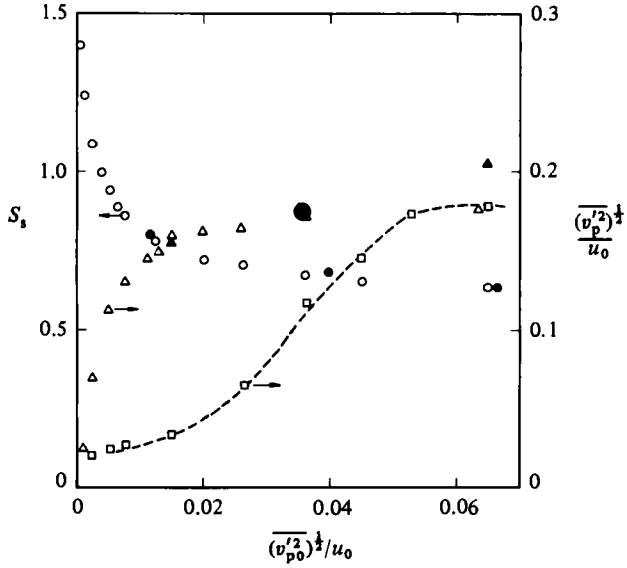

FIGURE 21. Intensities of maximum periodic v' constituents at x_s and saturation Strouhal number S_s versus excitation amplitude: ○, △, basic frequency; □, subharmonic frequency (both at disturbed excitation condition); filled symbols, 'clean' condition.

The intensity distribution of the first harmonic ($2f_0$) and of the subharmonic ($\frac{1}{2}f_0$) are presented in figures 19 and 20 respectively. For weak excitation their levels remain approximately one order of magnitude below the intensity of the basic frequency. For higher excitation amplitudes at the disturbed condition the subharmonic intensities in particular increase considerably, reaching maxima equal to those of the basic frequency, thus initiating and indicating the pairing process, which indeed is only observed in those cases where the intensity of the subharmonic locally exceeds

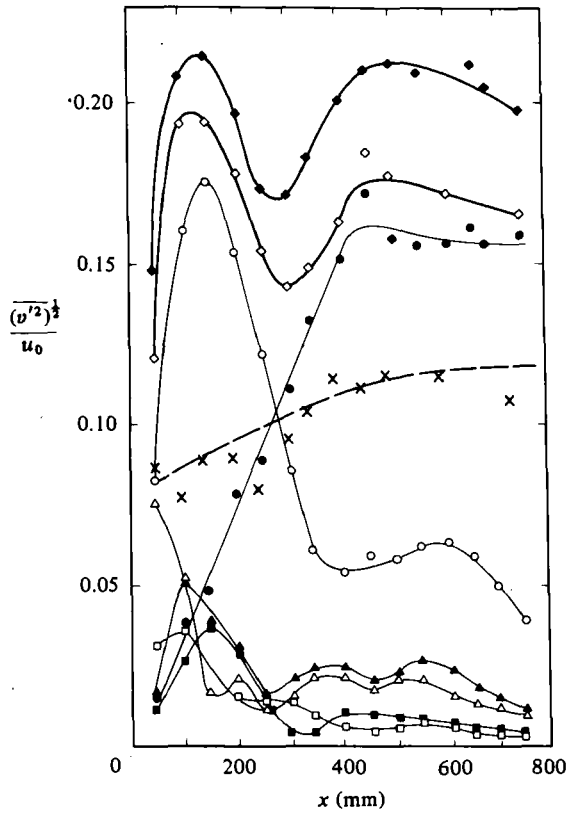

FIGURE 22. Periodic constituents of v' fluctuations at $y = 0$ for $f_0 = 30$ Hz and $(v_{p0})'/u_0 = 0.065$ versus x: ●, 15 Hz; ○, 30 Hz; ▼, 45 Hz; ▽, 60 Hz; ■, 75 Hz; □, 90 Hz; ◆, overall intensity $(v)'/u_0$ (measured); ◇, total intensity of periodic constituents; ×, intensity of non-periodic fluctuations $(v'^2/u_0 - v'^2/u_0)^{\frac{1}{2}}$; ——, neutral distribution (measured).

that of the basic (see also Ho & Huang 1982). At the clean excitation condition, where pairing is not observed, the intensity of the subharmonic always remains an order of magnitude below that of the basic.

In figure 21 magnitudes and locations of the maxima of periodic intensities are plotted versus relative excitation amplitude. Included are some data for strong excitation with clean excitation condition, which corroborate the observation that for weak excitation the condition at the trailing edge is of no consequence for the flow development (i.e. if flow separation remains fixed to the trailing edge).

For high excitation these curves appear to approach the asymptotic values $S_s \rightarrow 0.6$ and $(v_p)'/u_0 \rightarrow 0.2$.

For the case of strongest excitation ($(v_{p0})'/u_0 = 0.065$) the overall intensity of v' is plotted together with the intensity distributions of all periodic constituents found in the spectra for $y = 0$ versus x in figure 22. The maximum at basic frequency indicates the formation of the basic vortices (first pairing). The maximum of the subharmonic at about the downstream distance marks the formation of vortices with frequency $\frac{1}{2}f_0$ (second pairing – see also Ho & Huang 1982). This interpretation is supported by the smoke photographs on figure 8. Subtraction of the periodic energy from the overall v' energy yields the random constituent. It is somewhat surprising that the distribution thus obtained – with all due reservation for its accuracy – is

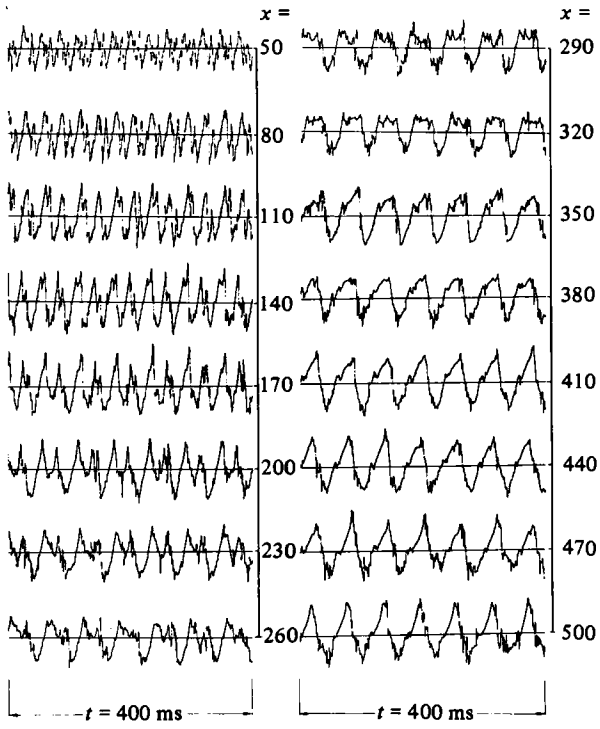

FIGURE 23. v' signal at different stations along x; $y = 0, f_0 = 30$ Hz, $(v_{p0})'/u_0 = 0.065$.

very close to the intensity distribution of the neutral flow, which seems to indicate that the random part of the turbulence remains essentially unaffected by the excitation. This appears to be in contradiction to other findings, but no explanation can be given at this point. Indeed it must be expected that in general the fine-grained turbulence is strongly influenced by the large-scale motions where turbulent laminae are distorted by being rolled up in a large vortex structure.

The regularity of the flow at strong excitation is demonstrated by the signal traces at $y = 0$ and various x-positions and at $x = 150$ (basic saturation length) across the flow, as shown in figures 23 and 24.

The stages described are easily identified and – as in the smoke photographs – considerably stronger determinism is observed on the high-velocity side. According to expectation, the behaviour of the flow shows close resemblance to the laminar shear layer under similar conditions, as, for example, investigated by Freymuth (1966) and by Miksad (1972).

3.2.3. *Limitations*

Provided the loudspeaker system will produce a pure sine wave at all desired frequencies, an upper frequency limit is introduced by the finite thickness of the separating boundary layer at trailing edge. Thus in the present experiments the amplification curve for 100 Hz no longer follows the similarity distribution in figure 25. Figure 16 shows that for this frequency saturation is reached already close to the trailing edge, where the characteristics of the separated boundary layer are still dominant. For $f_0 > 180$ Hz, x_s becomes negative. This frequency then would no longer experience amplification.

A lower limit for the excitation frequency is given by the size of the test section.

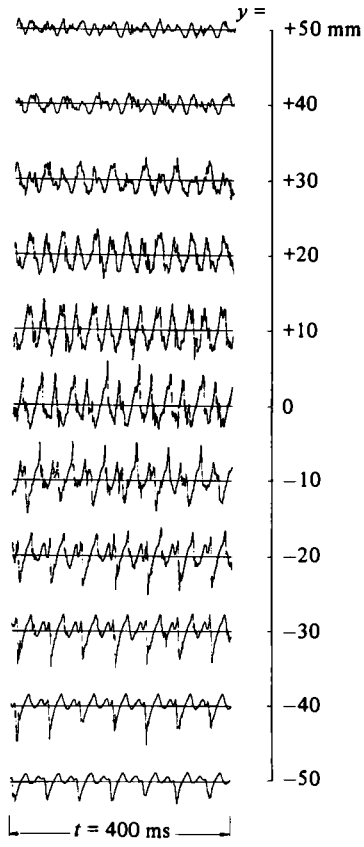

FIGURE 24. v' signal at various y-positions; $x = 150$ mm, $f_0 = 30$ Hz, $(v_{p0})'/u_0 = 0.065$.

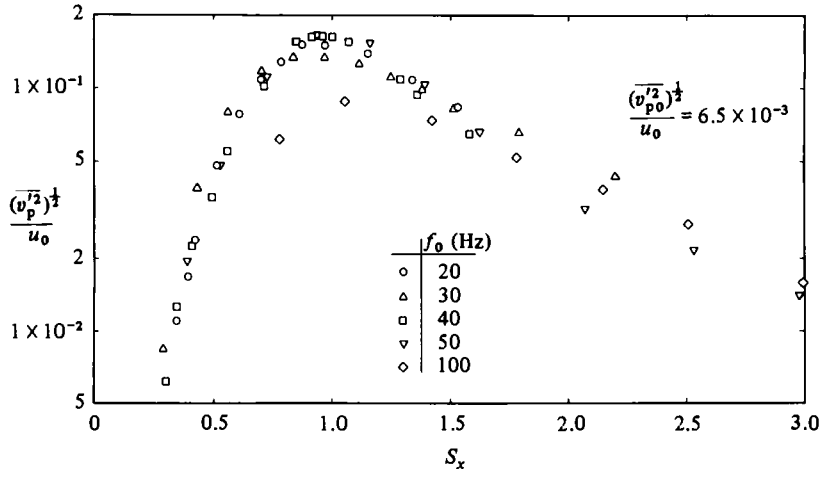

FIGURE 25. Frequency dependence of amplification.

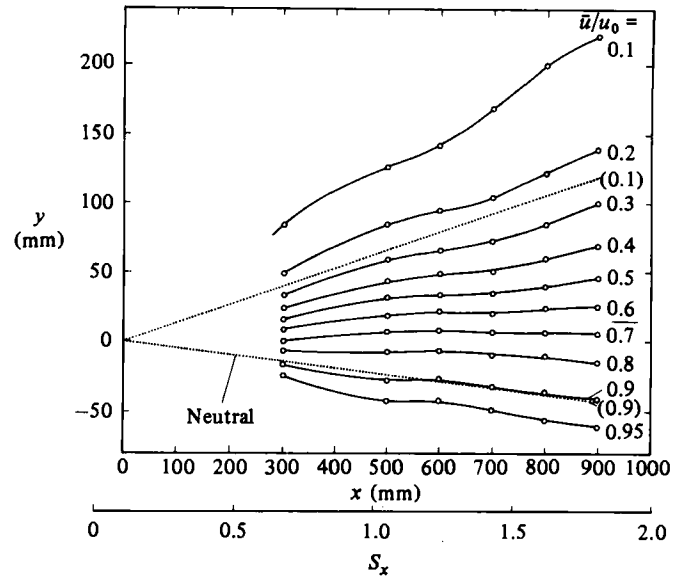

FIGURE 26. Mean-velocity isotachs for $(v_{p0})'/u_0 = 0.0065$ (weak excitation).

Not only might the interesting phenomena already be outside of the test section at very low frequencies (their downstream location being inversely proportional to f_0), but the proximity of the sidewalls may affect the flow by three-dimensional effects, while the bottom wall will increasingly influence the stability behaviour of the flow (modified boundary conditions) with increasing distance from the trailing edge, i.e. for decreasing frequencies (see also Wood & Bradshaw 1982).

4. Results: mean flow and turbulence characteristics

4.1. *Mean-flow development and entrainment*

The consequence of excitation on the mean quantities of turbulent shear layers has been described previously (e.g. Fiedler *et al.* 1981; Oster & Wygnanski 1982; Ho & Huang 1982). While the mean-velocity profiles, apart from being widened, essentially retain their shape except for very strong excitation (Wygnanski, Oster & Fiedler 1979), the excitation effect becomes visible in the isotach plots. Figures 26 and 27 juxtapose isotach distributions for weak excitation ($(v_{p0})'/u_0 = 0.0065$) and strong excitation ($(v_{p0})'/u_0 = 0.065$), where the isotachs for $u/u_0 = 0.1$ and 0.95 of the neutral flow are included for comparison. In contrast with the well-known behaviour at weak (i.e. 'clean') excitation, we observe at strong excitation two regions of steep growth, the first one at $S_x \approx 0.25$, indicating the formation of vortices at basic frequency (first pairing), the second at $S_x \approx 1$, indicating the formation of vortices at subharmonic (second pairing). The subsequent maxima of width are at the positions of maximum vortex strength. This course of events is also partly seen in the smoke photographs on figure 8. The strong influence of the vortices on the spread is particularly obvious from the emergence of slightly negative local growth rates, where the overall production is negative (see Takaki & Fiedler 1980).

Obviously the step-like increase of spread is always a consequence of vortex formation irrespective of whether pairing takes place or not. In these and the

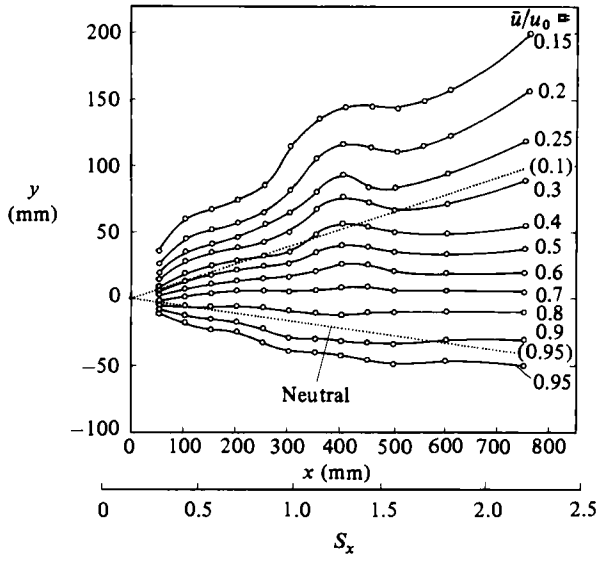

FIGURE 27. Mean-velocity isotachs for $(v_{p0})'/u_0 = 0.065$ (disturbed strong excitation).

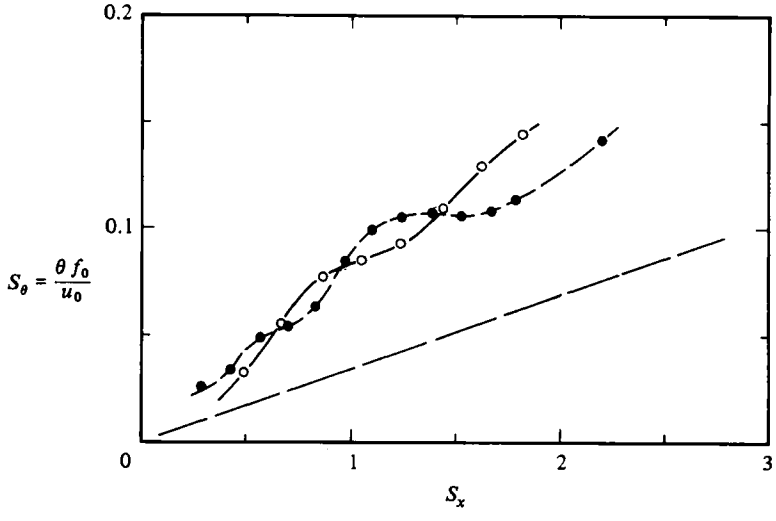

FIGURE 28. Shear-layer spread: ○, weak excitation; ●, strong excitation; ------, neutral flow.

following diagrams the lateral coordinate y is retained, since similarity coordinates do not apply.

The spread rate for the two cases is shown in figure 28. Surprisingly the mean spread rate is approximately the same for both cases, being about twice that of the neutral flow.

The spread of the shear layer is accompanied by entrainment of potential fluid from both sides. The mechanism of entrainment becomes particularly clear in the excited flow, where the potential fluid is rolled in on the leesides of the vortices. This is seen in the photographs on figure 6.

Figure 6(*a*) shows entrainment fluid as a dark region behind the second vortex.

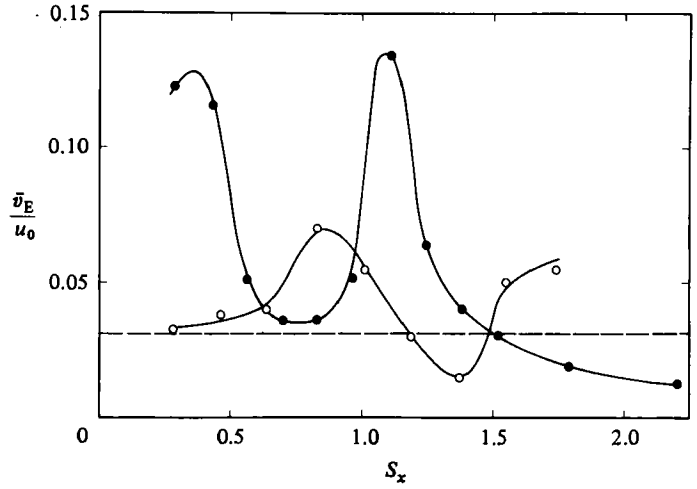

FIGURE 29. Entrainment velocities versus downstream position S_x for weak (○) and strong (●) excitation; – – – –, neutral flow.

It reaches far into the shear layer and is incorporated only on the other side. In figure 6(*b*) the entrainment flow is marked by smoke. Again we see the entrained fluid as a connected filament reaching far into the vortex. Thus the fully developed vortex appears to be quasi-laminated, and diffusion becomes a dominating factor only in the decay region (see also figure 10). At the same time small vortices appear on the periphery of the vortex. They may originate from the instability of the spooled-up laminae, which in fact are stabilized to some extent by their curvature.

On the zero-velocity side the entrainment flow is sucked into the turbulent regime from the ambient. We therefore measure a velocity towards the flow. On the high-velocity side the entrainment mechanism is somewhat different: there is no entrainment velocity in the potential flow, but the turbulent regime incorporates potential fluid by 'eating' into it. The flow rate entrained on the high-velocity side is approximately 2 times larger than on the zero-velocity side for the neutral shear layer. This ratio then becomes a function of x in the excited case, depending on the vortex development. Figure 29 shows entrainment velocities on the zero-velocity side versus S_x as obtained by integration of the mean-velocity profiles. The maxima are associated with the positions of strongest growth rates, demonstrating that pairing is not essential for entrainment. (Integration was performed only down to $u/u_0 = 0.1$, since at the outer edge of the flow measurements become increasingly uncertain).

4.2. *Turbulence quantities*

Longitudinal and transverse overall fluctuation-intensity distributions were measured for weak and strong excitation at various positions downstream. The weak-excitation case was measured with $f_0 = 20$ Hz, the strong-excitation case with $f_0 = 30$ Hz. The results may be directly compared by conversion of the respective x-position by the similarity relation

$$x_{f_{01}} = (x_{f_{02}} - x_0^*) f_{02}/f_{01} + x_0^*.$$

This has been verified by a number of test measurements at various frequencies, some of which are presented in figure 25.

Figures 30 and 31 give the $(u)'$ and $(v)'$ distributions for weak excitation at various x-positions. Distributions for the neutral flow measured at the farthest downstream

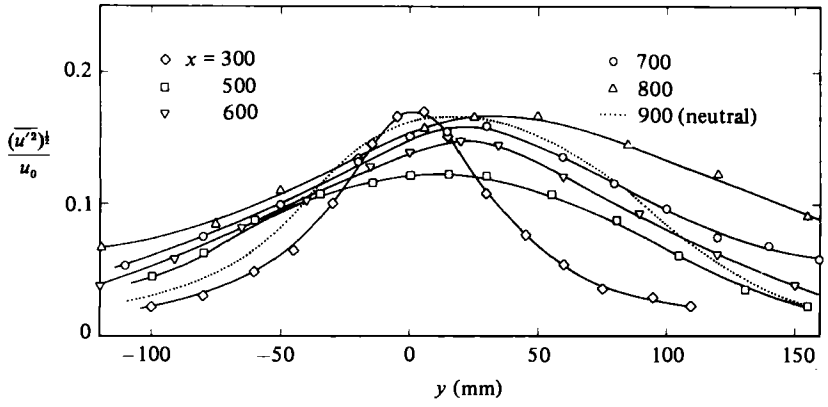

FIGURE 30. u' overall intensity profiles in weakly excited flow ($(v_{p0})'/u_0 = 0.0065$) at different x-positions.

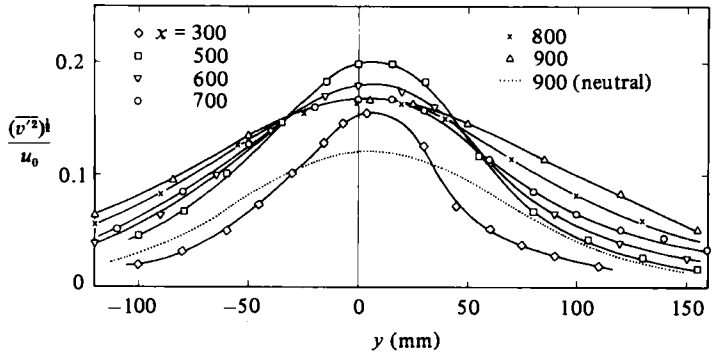

FIGURE 31. v' overall intensities in weakly excited flow.

position are included for comparison. Figures 32 and 33 show the corresponding distributions for the strongly excited case (disturbed condition).

While for weak excitation the distributions themselves, apart from being wider, retain their shape, resembling skewed Gaussian distributions with shifted maximum positions, we find a more complicated pattern at strong excitation. There particularly at the positions $x = 50$ mm and $x = 300$ mm the v' distribution appears to have two maxima, while at the same position the u' distributions are well-behaved, their maxima exceeding the natural value. From smoke photographs these locations are identified by considerable vertical dislocations preceding the pairing process. A situation where vortices appear in a staggered fashion, is likely to produce a strong u' maximum at the centerline and a double maximum of the v' fluctuations at approximately the vertical positions of the vortex cores. This is in contrast with a single row of vortices, which, when existing over a sufficient fetch as in a two-stream layer, will produce a strong v' maximum on the centreline and a double maximum of $(u)'$ at approximately the outer periphery of the vortices (see e.g. Oster & Wygnanski 1982).

Shear-stress distributions were measured only for the weakly excited case. They are shown in figure 34. The values for small x exceed the neutral curve in the region of vortex formation and are well below the latter for $x > x_s$ (decay region with

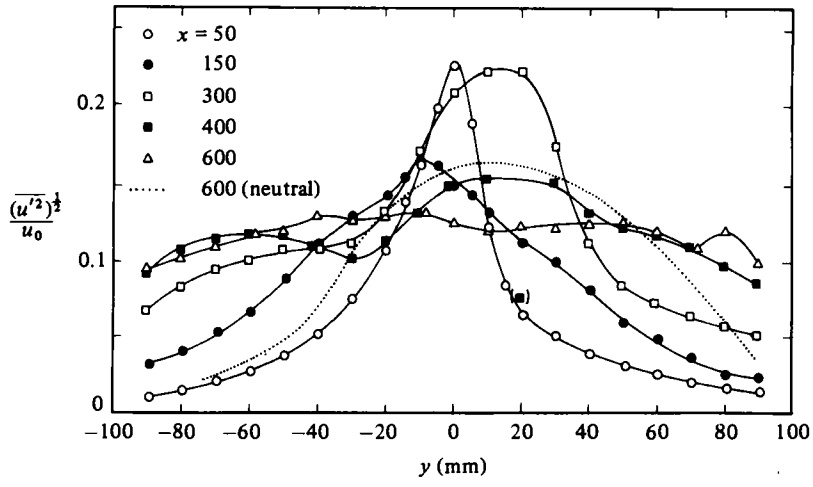

FIGURE 32. u' overall intensities at strong excitation ($(v_{p0})'/u_0 = 0.065$).

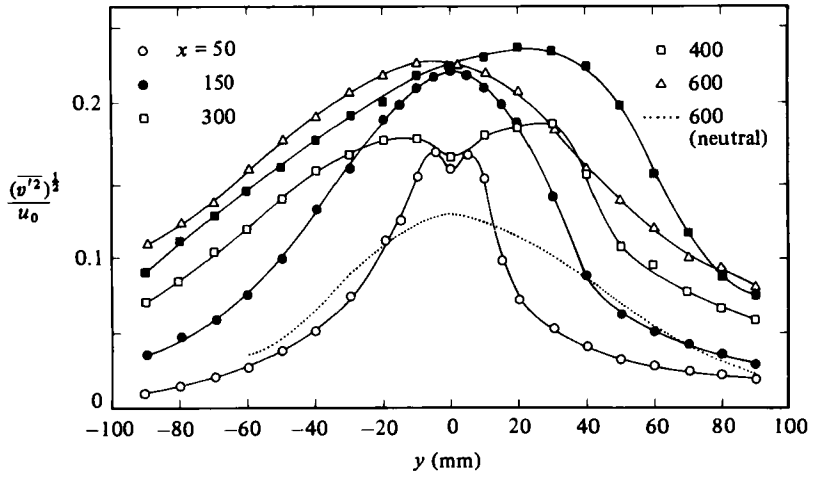

FIGURE 33. v' overall intensities at strong excitation.

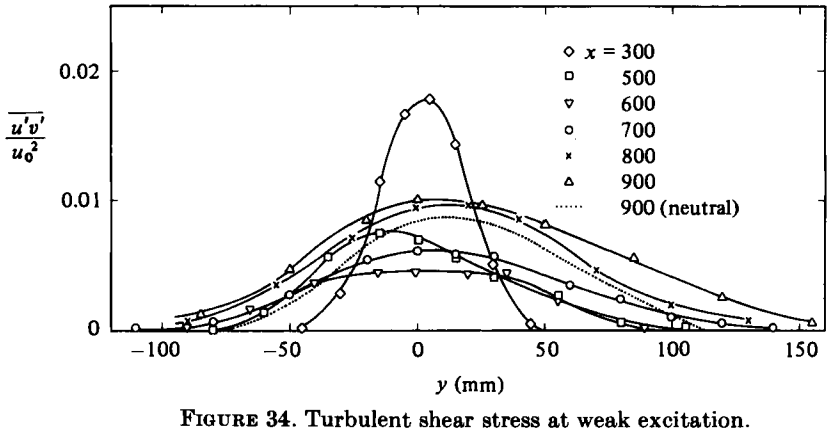

FIGURE 34. Turbulent shear stress at weak excitation.

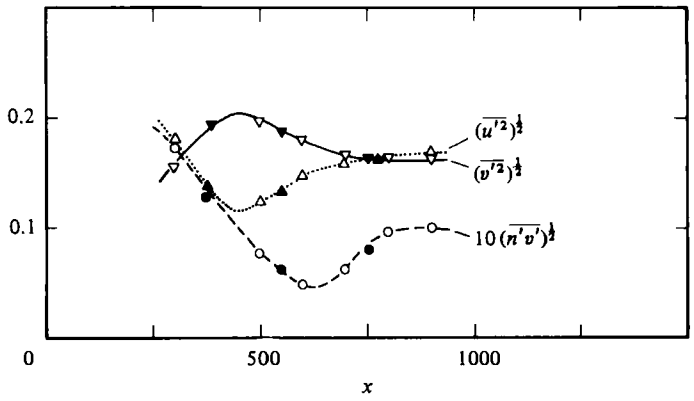

FIGURE 35. Longitudinal development of $(u_p)'(v_p)'$ and $(uv)'_p$ at $y = 0$: open symbols, $f_0 = 20$ Hz; full symbols, $f_0 = 30$ Hz, converted to 20 Hz (weak excitation).

negative $(uv)'_p$. From the measurements of Wygnanski *et al.* (1979) we know that for strong excitation even negative values of $(uv)'$ are found.

For better understanding, the axial development of the maximum values of the turbulence intensities and the shear stress as obtained from the previous figures (weak excitation) are presented in figure 35. These curves also include measurements at 30 Hz, where the conversion relation was applied, thus serving as additional proof for the general similarity. One particular aspect deserves mention: while it seems obvious that the turbulent intensity is increased in the excited flow by approximately its periodic constituent – as is indeed observed for the v' component – the reduced u' intensity at certain flow positions is more difficult to understand. A possible explanation may be as follows. A considerable part of the low-frequency random u' fluctuation energy in the neutral flow is caused by large-scale motions (coherent structures) with considerable vertical jitter. In the excited flow these motions are stabilized – most strongly at x_s – and their vertical dislocations minimized. The consequence may then be the suppression of the low-frequency u' fluctuations in the central region, as is particularly pronounced in the two-stream layer (Oster & Wygnanski 1982). Clearly this effect is different from the suppression observed for excitation frequencies an order of amplitude higher than those used in the present work by Zaman & Hussain (1981). In their case the excitation acted on the laminar/turbulent transition of an initially laminar shear layer, influencing the turbulence structure a long way downstream.

Another interesting point is the vertical dislocation of the intensity and shear-stress maxima. There we find considerable strong shifts in the $(u)'$ and the $(uv)'$ distributions, while the $(v)'$ maxima essentially remain at $y = 0$.

The shear-stress correlation is generally found to be around 0.45 for stochastic turbulence and monotonic profiles. On the axis of the neutral shear layer a value of 0.43 was indeed determined. In the presence of periodic vortices this value undergoes strong variations, reaching a maximum of 0.70 ahead of x_s, where it goes through the neutral value to a minimum at some position downstream and then back to 0.43. This may be explained by superposition of the deterministic and the stochastic constituents.

5. Summary and discussion

The neutral-plane shear layer is unstable for periodic perturbations introduced at the trailing edge. The perturbation wave is amplified along x, forming two-dimensional vortices of elliptical cross-section. The ratio of the major axes of the cross-sections of the fully developed vortex is approximately 1.8, which is in good agreement with theoretical values of Saffman (1980) and Jimenez (1980). The rate of amplification of the perturbation is highest at the onset of vortex formation (stability curve). It is zero at the saturation point x_s. At stations further downstream the amplification rate is negative (decay). The phenomenon is (ideal test conditions provided) frequency-dependent only inasmuch as the downstream position of saturation x_s is inversely proportional to the perturbation frequency. The total rate of amplification depends on the strength of excitation. It reaches a maximum of around 53 for $(v_{p0})' \to 0$. At saturation point the periodic energy constituent approaches a saturation value for strong forcing, which is of the order of 70 % of the total lateral fluctuation energy.

It was observed that the sequence of periodic events in the flow is sensitive to the separation condition at the trailing edge. When forcing is applied such that the separation remains at all times fixed to the trailing edge only vortices of basic frequency are formed. After the saturation point the periodic energy decays exponentially, while the vortices themselves lose coherence without pairing. The decay of periodicity is rather weak, and return to the neutral state may be expected only at a great distance.

When, on the other hand, at strong forcing the separation point is no longer fixed to the trailing edge but moves periodically upstream, a stable condition of repeated pairing may set in.

Diffusion by small-scale random motion inside the vortices during their formation appears to be comparatively weak. It becomes a major factor only in the decay region. Formation of vortices – be it with or without pairing – is always accompanied by strong increase of spread and thus of entrainment. After saturation the spread rate is strongly decreased and may even become negative. In the mean, however, excited flows always experience considerably stronger spread than the natural. It is approximately twice the neutral value and surprisingly independent of forcing amplitude. At saturation point the longitudinal fluctuation level goes through a minimum, while the lateral fluctuations reach their highest values. The turbulent shear stress has a maximum at vortex formation (maximum amplification) and a minimum at the beginning of decay.

A number of observations may be related to the natural shear layer.

The life cycle of a triggered structure (see Fiedler *et al.* 1981) exhibits essentially two phases.

(1) *Excitation of vortex.* The vortex is backward-leaning. It receives energy from the mean flow, which shows increased growth rate, increased entrainment and high values of $(uv)'$. At the point of maximum energy the structure is deformed such that the vortex becomes forward-leaning.

(2) *Decay of vortex.* The vortex is forward-leaning. Energy is returned to the mean flow. The mean spread, entrainment and turbulent shear stress are reduced and below the average natural values. Subharmonics leading to pairing are often suppressed to such an extent that the vortex will decay before pairing may set in.

In the natural case, on the other hand, pairing is observed as a common feature of structural development. Onset of pairing and the subsequent development of the

	Natural (Hernan & Jimenez 1982)	Excited (Mensing 1981)
Vortex geometry a/b	1.84	1.8
Wavelength $\Lambda/\lambda_u(x-x_0)$†	0.578	0.56
Convection velocity $u_c/(u_1+u_2)$†	0.49	0.5

† $\lambda_u = (u_1-u_2)/(u_1+u_2)$; here $u_1 = u_0, u_2 = 0$.

TABLE 1

amalgamated structure show, however, the same course of events as the single structure during its amplification phase and thus have the same effects on the mean flow, e.g. increase of spread, shear stress and entrainment.

It therefore appears of little relevance whether a vortex in its amplification phase is formed by a rolled-up vortical layer or of two vortices via their amalgamation. Only the geometrical situation is important for its influence on the flow and this is characterized by a 'forward-leaning position' (Takaki & Fiedler 1980).

Comparison of the present findings with the high-speed film analysis of a natural shear layer by Hernan & Jimenez (1982) shows good agreement in some comparable parameters as shown in table 1.

We have found the envelope spectrum of the coherent (periodic) constituent to be universal in amplitude and frequency (figure 15). It may thus be thought of as a probability density distribution for large-scale structures versus frequency at any position on the axis of a neutral layer, i.e. the spectral part of the coherent structures in the natural shear-layer spectrum. Comparison with the neutral spectrum provides us with a crude estimate of the coherent energy content of the natural flow. The approximately 20 % thus obtained is in good agreement with the value proposed by Browand & Ho (1983).

Hussain (1983) obtained peak r.m.s. values in the average coherent structure of the natural one-stream shear layer of order 3 % of the freestream velocity. We find comparable energy conditions for the lowest excitation amplitude which fits perfectly into the general spectrum curve (figure 15). This supports the above reasoning. Hussain's result should, however, not be misinterpreted: The strongest structures educed at a certain position are only those at the apex of their life cycle, i.e. at their energetic maximum. They must therefore be expected to be of small, possibly insignificant, energy content as compared with the overall turbulence, while on the other hand the total fraction of coherent turbulent energy at the point of observation over all frequencies may well be of the order of 20 %.

This investigation was substantially supported by Deutsche Forschungsgemeinschaft.

REFERENCES

BRADSHAW, P. 1966 The effect of initial conditions on the development of a free shear layer. *J. Fluid Mech.* **26**, 225–236.

BROWAND, F. K. & HO, C.-M. 1983 The mixing layer: an example of quasi two-dimensional turbulence. *J. Méc. Numéro Spécial: Turbulence & idimensionelle*, pp. 99–120.

BROWAND, F. K. & TROUTT, T. 1980 A note on spanwise structure in the two-dimensional mixing layer. *J. Fluid Mech.* **97**, 771.

BROWN, G. & ROSHKO, A. 1974 On density effects and large structure in turbulent mixing layers. *J. Fluid Mech.* **64**, 775–816.

FIEDLER, H., DZIOMBA, B., MENSING, P. & RÖSGEN, T. 1981 Initiation, evolution and global consequences of coherent structures in turbulent shear flows. In *The Role of Coherent Structures in Modelling Turbulence and Mixing* (ed. J. Jimenez). Lecture Notes in Physics, vol. 136, pp. 219–251. Springer.

FREYMUTH, P. 1966 On transition in a separated laminar boundary layer. *J. Fluid Mech.* **25**, 683–704.

HO, C.-M. & HUANG, L.-S. 1982 Subharmonics and vortex merging in mixing layers. *J. Fluid Mech.* **119**, 443–473.

HUSSAIN, A. K. M. F. 1983 Coherent structures – reality and myth. *Phys. Fluids* **26**, 2816–2850.

HUSSAIN, A. K. M. F. & ZEDAN, M. F. 1978*a* Effects of the initial condition on the axisymmetric free shear layer: effects of the initial momentum thickness. *Phys. Fluids* **21**, 1100–1111.

HUSSAIN, A. K. M. F. & ZEDAN, M. F. 1978*b* Effects of the initial condition on the axisymmetric free shear layer: Effects on initial fluctuation level. *Phys. Fluids* **21**, 1475–1481.

HERNAN, M. A. & JIMENEZ, J. 1982 Computer analysis of a high-speed film of the plane turbulent mixing layer. *J. Fluid Mech.* **119**, 323–345.

JIMENEZ, J. 1980 On the visual growth of a turbulent mixing layer. *J. Fluid Mech.* **96**, pp. 447–460.

KORSCHELT, D. 1980 Experimentelle Untersuchung zum Wärme- und Stofftransport im turbulenten ebenen Freistrahl mit periodischer Anregung am Düsenaustritt. Dissertation Hermann-Föttinger-Institut, TU Berlin.

MENSING, P. 1981 Einfluß kontrollierter Störungen auf eine ebene turbulente Scherschicht. Dissertation Hermann-Föttinger-Institut, TU Berlin.

MENSING, P. & FIEDLER, H. 1980 Eine Methode zur Sichtbarmachung von hochturbulenten Luftströmungen mit großen Reynoldszahlen. *Z. Flugwiss. Weltraumforsch.* **4**, 366–369.

MICHALKE, A. 1971 Instabilität eines kompressiblen runden Freistrahls unter Berücksichtigung des Einflusses der Strahlgrenzschichtdicke. *Z. Flugwiss. Weltraumforsch.* **19**, 319.

MIKSAD, R. W. 1972 Experiments on the nonlinear stages of free-shear-layer transition. *J. Fluid Mech.* **56**, 695–719.

MIKSAD, R. W. 1973 Experiments on nonlinear interactions in the transition of a free shear layer. *J. Fluid Mech.* **59**, 1–21.

OSTER, D. & WYGNANSKI, I. 1982 The forced mixing layer between parallel streams. *J. Fluid Mech.* **123**, 91–130.

SAFFMAN, P. G. 1980 Coherent structures in turbulent flow. In *The Role of Coherent Structures in Modelling Turbulence and Mixing* (ed. J. Jimenez). Lecture Notes in Physics, vol. 136, pp. 1–9. Springer.

SMITH, A. M. O. & CLUTTER, D. W. 1957 The smallest height of roughness capable of affecting boundary layer transitions in low-speed flow. *Douglas Aircraft Co. Inc., Rep.* ES 26803.

TAKAKI, R. & FIEDLER, H. 1980 A phenomenological model of the organized vortex in the two-dimensional mixing layer. *IUTAM Symp. Yugoslavia.*

WEI, Z.-L., NIU, Z.-N. & MA, W.-J. 1982 The disturbances affect Brown–Roshko structures in plane mixing layer. In *Structure of Complex Turbulent Shear Flow, IUTAM Symposium Marseille* (ed. R. Dumas & L. Fulachier), pp. 137–145.

WOOD, D.-H. & BRADSHAW, P. 1982 A turbulent mixing layer constrained by a solid surface. Part 1. Measurements before reaching the surface. *J. Fluid Mech.* **122**, pp. 57–89.

WYGNANSKI, I., OSTER, D. & FIEDLER, H. 1979 A forced, plane, turbulent mixing layer; a challenge for the predictor. In *Proc. 2nd Symp. on Turbulent Shear Flows, London.*

ZAMAN, K. B. M. Q. & HUSSAIN, A. K. M. F. 1981 Turbulence suppression in free shear flows. *J. Fluid Mech.* **103**, 133–150.